Reactive transport modelling of concrete subject to de-icing salts and atmospheric carbonation

Meijie Xie, Patrick Dangla, Kefei Li

Materials and Structures (2021)54:240
https://doi.org/10.1617/s11527-021-01835-2

ORIGINAL ARTICLE

Reactive transport modelling of concrete subject to de-icing salts and atmospheric carbonation

Meijie Xie · Patrick Dangla · Kefei Li

Received: 2 September 2021 / Accepted: 30 November 2021

Abstract This paper treats the chloride ingress in concrete subject alternatively to de-icing salts and atmospheric carbonation through a reactive transport model. The general framework of reactive transport model is reviewed for its treatment of the carbonation reactions, the CO_2 and ionic transport and the dissolution equilibrium between solid and liquid phases. Then the model is applied to typical frost climates with application of de-icing salts and the environment conditions are idealized as yearly-based cycles having evenly distributed rainy and snowy events with drying periods in between. Comprehensive parametric study is performed on the impact of climate parameters and concrete properties, and obtains the following observations: (1) the determinant climate factor for chloride ingress is the intensity of de-icing salts application and relative humidity of drying periods plays a secondary role; (2) considering carbonation is to globally limit the chloride ingress mainly due to the decrease of chloride diffusivity by pore filling after concrete carbonation; (3) the moisture boundary conditions on concrete surface should take into account the wetting by rainy events otherwise the surface washing of chlorides will be omitted.

Keywords De-icing salt · Concrete · Chloride ingress · Carbonation

1 Introduction

De-icing salts containing chlorides, e.g. sodium chloride and calcium chloride, are widely applied to melt snow on pavements in winter [1]. The massive application of chloride-based de-icing salts bring forth several major durability problems for reinforced concrete: the surface scaling by de-icing salts [2, 3], the chemical damage by magnesium/calcium chlorides [4] and the corrosion of embedded reinforcement bars by chloride ingress [5]. For the latter, the main durability barrier is the concrete cover, which is specified in various design codes and standards for its resistance to chloride ingress and its thickness [6–8]. However, accurate modelling prediction is still necessary to improve the reliability of durability design and maintenance for concrete structures and elements subject to de-icing salts.

Conceptually, the application of de-icing salts is a seasonal event, i.e. highly correlated to the atmospheric frost and precipitation (snow). Thus, the

M. Xie · K. Li (✉)
Department of Civil Engineering, Tsinghua University, Beijing 100084, People's Republic of China
e-mail: likefei@tsinghua.edu.cn

M. Xie
e-mail: majorthu2016@foxmail.com

P. Dangla
Navier, Ecole des Ponts, Univ. Gustave Eiffel, CNRS, Marne-la-Vallée, France
e-mail: patrick.dangla@ifsttar.fr

Published online: 13 December 2021

concrete elements, such as RC pavements, are subject alternatively to de-icing salts in snowy season(s) and to atmospheric CO_2 during other periods. The clear description of such alternative action necessitates the knowledge of both chloride ingress through carbonated concrete and carbonation of chloride-borne concrete, and the appropriate description of boundary conditions as well. So far, efforts have been dedicated to the synergetic effect of chloride ingress and carbonation on the long-term durability of reinforced concretes. The complex behaviours of chloride ingress have been quantified through multi-field models combining the finite element method and thermodynamic software (GEMS) [9, 10]. Zhu et al. [11] built a probabilistic model to describe the combined actions of carbonation and chloride ingress in reinforced concrete structures with changing boundary conditions for environmental aggressive agents. Shen et al. [12] conducted simulations of unsaturated concrete under marine environments and demonstrated the carbonation impact on chloride ingress through debinding of chlorides. Xie et al.[13] applied a reactive transport model to concurrent chloride ingress and carbonation with no strong moisture transport on the boundary and indicated the global promoting nature of carbonation for corrosion risk for embedded steel. The studies of de-icing salts through long-term field tests also attract attentions. The field tests are valued since the combined environmental effects on real structural concretes are included [14–16]. Tang and Lindvall [15] compiled data of chloride ingress profiles from concrete specimens exposed on Swedish conditions, including roads and highway bridges, used DuraCrete model [17] and ClincConc model [18] to simulate the chloride ingress, and considered the carbonation effects through the changed chloride binding capacity in near surface zone in ClincConc model. Kuosa et al. [16] compared field tests in Finland and laboratory experiments on multiple processes of freeze–thaw, carbonation and chloride ingress, and observed that laboratory specimens subject firstly to chloride migration tests have lower carbonation depths and specimens with pre-carbonated layer have larger the chloride migration depths.

Accordingly, accurate simulations of alternative actions of de-icing salts and carbonation should include both the deepened mechanisms, coupling chloride transport and carbonation, and the appropriate boundary conditions. The boundary conditions adopted so far are not representative for concrete surface, and the material-environment interaction at concrete surface should address the chloride deposit, atmospheric carbonation, and surface washing and drying. Following this need, the paper uses a recently developed reactive transport modelling for concurrent carbonation and chloride ingress [13], and quantifies the synergic effect of de-icing salts and CO_2 in the atmosphere under more elaborated boundary conditions of concrete surface. To this purpose, this paper is organized as follows: Sect. 2 gives a brief review on the reactive transport modelling and the description for boundary conditions; Sect. 3 analyses the impact of environmental conditions on the synergic effects; Sect. 4 performs parametric analysis of concrete intrinsic properties on the synergic effects; Sect. 5 discusses the impact of moisture conditions of concrete surface on chloride ingress; and the conclusion remarks are given in the end.

2 Reactive transport modelling: a review

The development and experimental validation of the reactive transport model have been presented in Xie et al. [13], and a brief description of the modelling framework is recalled in the following. Concrete is regarded as a reactive porous medium partially saturated by liquid phase of pore electrolytic solution containing multi-species. The pore saturation, s_L, is defined as the ratio between the liquid-occupied pore volume to the total pore volume. The gas phases in pores include vapour and dry air (containing CO_2), and the total gas pressure, p_G, is assumed to be constant, equal to the external atmospheric pressure p_{atm}. The CO_2 transport is driven by its concentration gradient following Fick's law,

$$\underline{w_{CO_2}} = -D^e_{CO_2(G)} \cdot \underline{\nabla c^G_{CO_2}} \tag{1}$$

where $D^e_{CO_2(G)}$ stands for CO_2 diffusivity in pore gas phases. In liquid phase, the advection of pore solution observes Darcy's law,

$$\underline{w_L} = \rho_w \underline{q_L} = -\rho_w \frac{k_{int}}{\eta_l} k_{rl} \underline{\nabla p_L} \tag{2}$$

Here $\underline{q_L}$ denotes the flow rate (m/s), k_{int} is the intrinsic permeability of concrete (m^2), k_{rl} stands for the relative permeability (-) and η_l the viscosity of fluid

(Pas). The flow of aqueous ions, w_i (kg/m^2/s), includes both advection and diffusion terms,

$$\underline{w_i} = c_i \underline{q_L} + \underline{J_i} \quad with\, \underline{J_i} = -D_i^e \left(\underline{\nabla c_i} + c_i \frac{z_i F}{RT} \underline{\nabla \psi} \right) \tag{3}$$

where $D^e{}_i$ is the effective diffusivity of ion species i (m^2/s), z_i the valence of ion species i, F the Faraday's constant (96,485 C/mol), R the ideal gas constant (8.314 J/K/mol), T the absolute temperature (K), and Ψ the electric potential (V). Note that the CO_2 diffusivity $D^e{}_{CO2(G)}$, the relative permeability k_{rl} and the ion diffusivity D_i^e all highly depend on the pore liquid saturation s_L, and their expressions will be detailed in later analysis.

During transport, the ions observe the global conservation of electric charge and the electroneutrality for pore solution [19],

$$\mathrm{div}\left(\underline{j}\right) = 0 \quad with\, \underline{j} = \sum_i z_i \underline{w_i} \tag{4}$$

$$\sum_i z_i c_i = 0 \tag{5}$$

The mass conservation of six elements, calcium (Ca), silicon (Si), carbon (C), chloride (Cl), potassium (K) and sodium (Na), is written as follows,

$$\frac{\partial n_A}{\partial t} = -div\, \underline{w}_A \quad with \quad A = Ca, Si, C, Cl, K, Na \tag{6}$$

The conservation of the total mass m_{tot} of representative elementary volume (REV) of concrete material writes,

$$\frac{\partial m_{tot}}{\partial t} = -div \underline{w}_{tot} \quad with \quad \underline{w}_{tot} = \underline{w}_L + \underline{w}_{va} + \underline{w}_{CO_2} \tag{7}$$

where $\underline{w}_{L,va,CO_2}$ stand for the flows of pore solution (liquid), water vapour (gas) and CO_2 (gas) respectively.

The equilibria exist between the solid phases and the aqueous ions in pores. The homogeneous reactions are governed by their respective equilibrium constants [13, 20], and for heterogeneous reactions, i.e. dissolution and precipitation of portlandite (CH), calcium silicate hydrates (C-S-H) and calcium carbonate $C\bar{C}$), the solubility products are given in Table 1 with a special treatment to the dissolution equilibrium for C-S–H [13]. Note that these constants are temperature dependent.

The physical effect of carbonation is described by the pore filling of calcite precipitation [22],

$$\Delta\phi = -V_{CH}\left(n_{CH} - n_{CH}^0\right) - V_{CC}\left(n_{C\overline{C}} - n_{C\overline{C}}^0\right) - \left(V_{CSH} n_{Si} - V_{CSH}^0 n_{Si}^0\right) \tag{8}$$

where $V_{CH,C\overline{C},CSH}, n_{CH,C\overline{C},CSH}$ stand for the molar volume (m^3/mol) and molar concentration (mol/m^3) of hydrates CH, C$\overline{\text{C}}$ and C-S–H.

The interaction between the solid phases and chlorides refers to the chloride binding (absorption) of solid phases. The adsorption of chlorides of concrete, before or after carbonation, is described by a Langmuir-type isotherm,

$$s_{\mathrm{Cl}}(c_{\mathrm{Cl}}) = \frac{\alpha_{\mathrm{Cl}}(\mathrm{C/S}) c_{\mathrm{Cl}}}{1 + \beta_{\mathrm{Cl}}(\mathrm{C/S}) c_{\mathrm{Cl}}} \tag{9}$$

with s_{Cl} standing for chloride binding capacity (mol/mol CSH). The impact of carbonation on the chloride binding is taken into account by linking the absorption coefficients α_{Cl}, β_{Cl} to the calcium to silicon ratio C/S of C-S–H [13]. The equilibrium between liquid and gas phases of water is described by the moisture sorption isotherm,

$$p_G \equiv p_{atm} : p_c(s_L) = p_G - p_L = -\rho_w \frac{RT}{M_w} \ln h \quad with \quad h = \frac{p_{va}}{p_{vs}(p_G, T)} \tag{10}$$

where h stands for the external relative humidity (%), ρ_w, M_w for the water density (kg/m^3) and molar mass of water (0.018 kg/mol), and $p_{va,vs}$ for the vapour pressure (Pa) and saturated vapor pressure (Pa) at a given gas pressure p_G (Pa) and temperature T (K). The capillary pressure p_c (Pa) in terms of pore saturation, or moisture characteristic curve, follows van Genuchten's model [23] and takes the following form [24],

$$p_c(s_L) = a\left(s_L^{-b} - 1\right)^{1-1/b} \tag{11}$$

with a, b as material parameters.

Under this general reactive transport framework, the carbonation and chloride ingress can be investigated in a multi-species context under prescribed boundary conditions. The model is solved through finite volume method with the open numerical platform Bil [25]. In the foregoing study [13], the model was applied to concurrent carbonation and

Table 1 Equilibrium solubility products of solid compounds at $T = 298.15$ K

Mineral	Dissolution reactions	logK
Portlandite	$CH \rightleftharpoons Ca^{2+} + 2OH^-$	− 5.2
Calcium carbonate	$C\overline{C} \rightleftharpoons Ca^{2+} + CO_3^{2-}$	− 8.48
Calcium and silicate hydrates	$C_xSH_z \rightleftharpoons xCa^{2+} + 2xOH^- + SiO_2^0 + (z - x)H_2O$	CH saturation index[21]

chloride ingress. In this study, simulations are performed for the alternative actions of de-icing salts and atmospheric carbonation on concrete surface.

3 Impact of environmental conditions of de-icing salts

3.1 Boundary conditions and material properties

The deposit of chlorides on concrete surface from application of de-icing salts results from the complex interactions between environment and concrete material. The average amount of de-icing salts applied on the roads of New York State (US), between 2002 and 2006, was estimated as much as 19.6×10^3 kg/km/lane per year [26]. The de-icing salts, once applied onto concrete surface, melt into a chloride solution of high concentration, if not saturated. This high concentration solution of chlorides can penetrate into concrete, and can be also washed off by raining, even sprayed up into surroundings [27]. To account for this complex condition, we divide the environmental actions on concrete surface into two periods on yearly basis: "snowy period" refers to the time in which frost actions are active and de-icing salts are applied, "rainy period" refers to the time without frost actions in which concrete surface is exposed to atmosphere. In this study, only sodium chloride (NaCl) is considered for de-icing salts.

In snowy period, the surface chlorides are quantified with respect to the snow and de-icing events, which are related closely to the local climate. During the snow melting, a saturated chloride solution is assumed to act on the concrete surface, i.e. 5.3 mol/L for NaCl salts. The duration of each snow melting event is estimated by the bare pavement regain time (BPRT), which is the elapsed time from de-icing salt application to the time when the bare pavement achieves 80% [28]. Hussain et al. [29] reported the average BPRT as 4.37 h and this value is rounded to 6 h in simulations. The number of snow events will be determined by local meteorological data, and between adjacent snow melting events the concrete surface is exposed to atmosphere with the average relative humidity and CO_2. In rainy period, the count of rain events is also determined by local meteorology, and each raining event is supposed to last for 4 h. Between the adjacent rainy events the concrete surface is exposed to atmosphere with average relative humidity and CO_2. The above boundary conditions of concrete surface are summarized in Table 2.

Two typical cities in China, Beijing and Harbin, are selected for simulations, noted as Case 1 and Case 2 respectively. Compared with Beijing, Harbin has longer winters, more snow and rainfall. Meteorological data, including average temperature and rainfall, are obtained from the observation stations of Beijing (1997–2010) and Harbin (1981–2010) [30]. Using the above division of snowy and rainy periods, the yearly environmental conditions are illustrated in Fig. 1 with rain and snow events count for atmospheric precipitation exceeding 10 mm and 1 mm respectively. For simplification, the rain (green) and snow (red) events are distributed evenly in the rainy and snowy periods respectively. In Fig. 1, Case 1 (Beijing) has average RH = 55% and counts 13 rain and 3 snow events while Case 2 (Harbin) has average RH = 65% and counts 15 rain and 8 snow events. For comparison purpose, a hypothetical case, Case 3, is set up using the same rain and snow counts as Case 2 but adopts the average RH = 55%. Also, for comparison purpose the thermal conditions are greatly simplified, taking 273.15 K for snowy period and 293.15 K for rainy period. The atmospheric CO_2 concentration is retained as 380 ppm for all year long, cf. Table 2.

This study retains an OPC concrete (OPC50-1) and OPC-FA concretes for the reactive transport simulations. This OPC concrete contains 330 kg/m^3 ordinary Portland cement as binder and has water to cement

Table 2 Boundary conditions for Case 1, Case 3(Case 2)

	Initial state	Rainy period		Snowy period	
	Concrete	Drying	Raining	Drying	Melting
RH (%)	75	55(65)	100	55(65)	100
Na^+ (mol/L)	0.07	10^{-10}	10^{-10}	5.3	5.3
Cl^- (mol/L)	10^{-10}	10^{-10}	10^{-10}	5.3	5.3
Temperature (K)	293.15	293.15	293.15	273.15	273.15
CO_2 concentration (ppm)	–	380	380	380	380

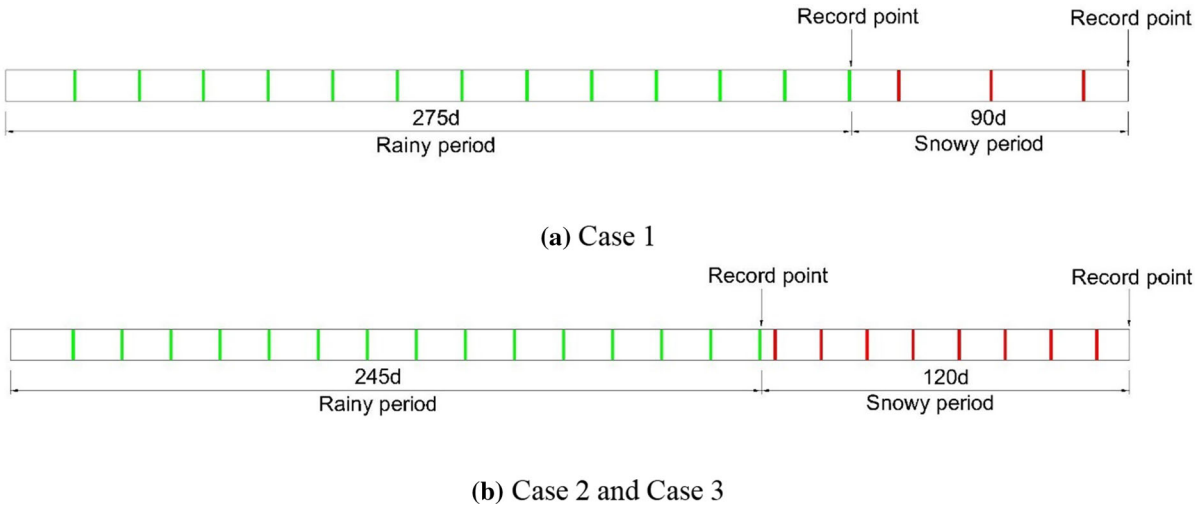

Fig. 1 Distribution of rain and snow events for simulation of concrete surface during 1 year ("Record point" means the time point of which the simulation results are to be presented.)

ratio of 0.5 while the OPC-FA concretes incorporate 0–20% fly ash (FA) in the binder [13]. The main properties of these concretes are given in Table 3.

3.2 Chloride ingress without carbonation

As a comparison basis, the chloride ingress is firstly simulated for Case 1–3 for a service life of 50 years without considering the atmospheric carbonation. The free chloride profiles are presented in Fig. 2 at different exposure ages for different record points in Fig. 1. The first feature of chloride profiles is the strong advection layer near the surface, around 0.8 cm, due to the alternative actions of snowy and rainy periods: during snowy periods the de-icing salts melt into chloride solution and ingress into the concrete, and during the rainy periods the penetrated chlorides are washed out by surface wetting during rain events (RH = 100%). Note that both the melting of de-icing salts and the rain event take intermittent patterns as indicated in Fig. 1. The drying durations in rainy period also contribute to the inflection of free chloride profiles through the pore saturation change near surface, but taking a secondary role. It is also noted that, during the same year, the free chloride profile after the snowy period augments just slightly compared to that after the rainy period in the depth beyond the advection depth.

Figure 3 compares the final profiles of free and total chlorides for Case 1–3 at the end of 50 years, revealing the impact of the local environmental conditions including the average relative humidity and the frequency of rain and snow events. It seems that the intensity of de-icing salts application, related to counts of snow events, determines the chloride ingress extent: Case 1, with less snow events compared to Case 2 and Case 3, has profiles notably below the other two cases. Case 3 has the same rain and snow counts as Case 2 but assumes a lower RH = 55% during the drying durations, leading to even higher chloride concentrations

Table 3 Properties for concretes used in the reactive transport simulations

Parameters/Properties	Value
Volume ratio of cement paste v_p (−)	0.275
Volume ratio of coarse aggregates v_{ca} (−)	0.420
Volume ratio of fine aggregates v_{fa} (−)	0.305
Initial CH content n^0_{CH} (mol/m^3), OPC concrete [13]	1187
Initial CH content n^0_{CH} (mol/m^3), OPC-FA concrete (0%FA) [13]	1085
Initial CH content n^0_{CH} (mol/m^3), OPC-FA concrete (10%FA) [13]	537
Initial CH content n^0_{CH} (mol/m^3), OPC-FA concrete (20%FA) [13]	63
Initial C-S–H content $n^0_{C\text{-}S\text{–}H}$ (mol/m^3), OPC concrete [13]	601
Initial C-S–H content $n^0_{C\text{-}S\text{–}H}$ (mol/m^3), OPC-FA concrete (0%FA) [13]	664
Initial C-S–H content $n^0_{C\text{-}S\text{–}H}$ (mol/m^3), OPC-FA concrete (10%FA) [13]	699
Initial C-S–H content $n^0_{C\text{-}S\text{–}H}$ (mol/m^3), OPC-FA concrete (20%FA) [13]	721
Initial porosity ϕ (−)	0.14
Intrinsic permeability k_{int} (10^{-21}m^2) [31]	2.4
Effective chloride diffusivity in saturated concrete D^e_{Cl} (10^{-12}m^2/s)	2.95
Tortuosity factor in ion diffusivity c (−) [13]	2.1
Tortuosity factor in ion diffusivity d (−) [13]	0.65
Ageing exponent of chloride diffusivity m (-), OPC concrete [17]	0.65
Ageing exponent of chloride diffusivity m (−), OPC-FA concrete [17]	0.66
Moisture characteristic curve parameter a (MPa) [32]	18.62
Moisture characteristic curve parameter b (−) [32]	2.275

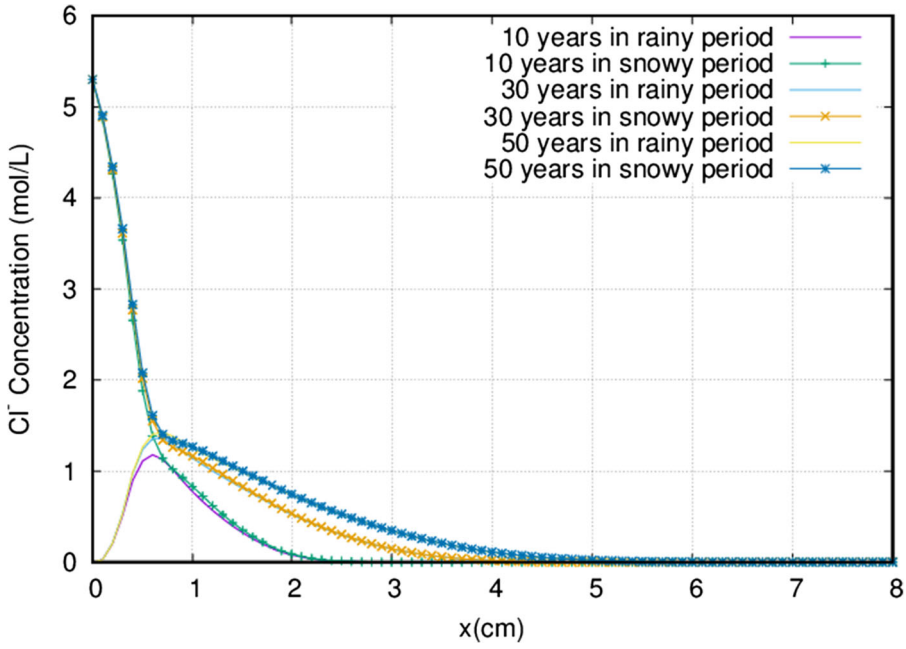

Fig. 2 Free chloride profiles of Case 2 at different exposure ages

than Case 2 within 2 cm from surface. This phenomenon is due to the stronger surface advection effects from the lower drying humidity (RH = 55%) in Case 3. Beyond the depth of 2 cm, Case 2 profiles become higher. An easier indicator would be the total chloride intake for the three cases after 50 years of

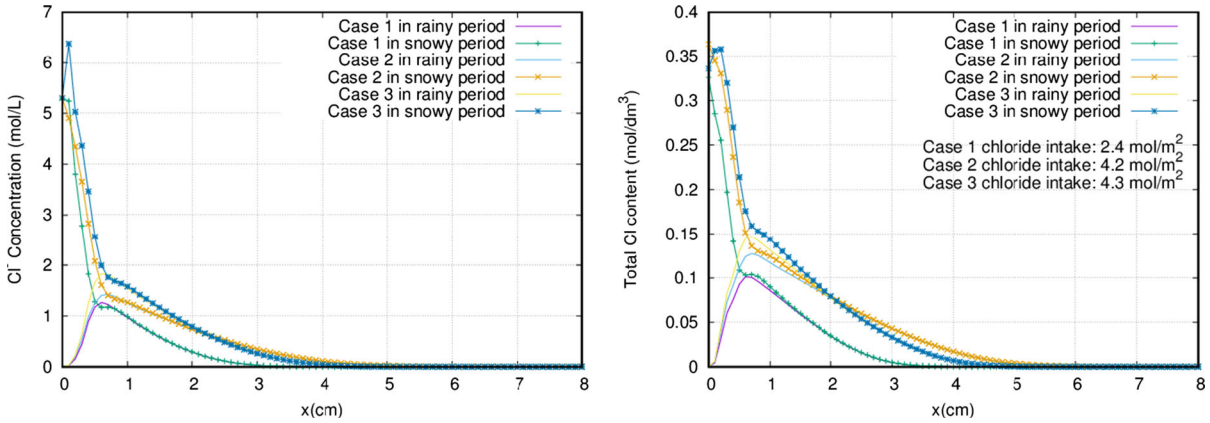

Fig. 3 Free chlorides (left) and total chlorides (right) of Case 1–3 in 50 years without carbonation

exposure: 2.4 mol/m^2, 4.2 mol/m^2 and 4.3 mol/m^2 for Case 1, 2 and 3 respectively, which are consistent with the profile analysis.

The chloride profiles depend strongly on the moisture transport in pores, and thus the pore saturation results are given in Fig. 4. It can be seen that the inflection position of pore saturation profiles is close to the advection depth of chlorides in Fig. 2, around 0.5 cm, i.e. less deeper than the advection depth of chlorides. The total water intake is calculated from the pore saturation profiles and the water gain within 10 cm depth at the end of 50 years is -0.77 kg/m^2, 0.28 kg/m^2, and -0.18 kg/m^2 for Case 1, 2 and 3 respectively. Thus, the concrete surface tends to lose water for Case 1 and Case 3, but gain water for Case 2. From the viewpoint of moisture transport Case 2 belongs to wetting-dominating cases, and Case 1 and Case 3 to drying-dominating cases. Figure 4 provides also the profiles of the concentration ratio Cl^-/OH^-, taken usually as an electrochemical indicator for steel corrosion initiation [33]. Taking $Cl^-/OH^- = 1.0$ as a rough criterion, the corrosion initiation depths are 2.3 cm (Case 1), 3.3 cm (Case 3) and 3.7 cm (Case 2). Accordingly, the order of importance for factors of corrosion risk is rather clear: first the intensity of de-icing salts application and then the environmental humidity.

3.3 Chloride ingress with atmosphere carbonation

During drying durations in both rainy and snowy periods, the concrete surface of elements, such as road pavements, is exposed to CO_2 in atmosphere thus susceptible to carbonation. The atmospheric CO_2 concentration is taken as 380 ppm [34], cf. Table 2, and the reactive transport model in Sect. 2 is used to

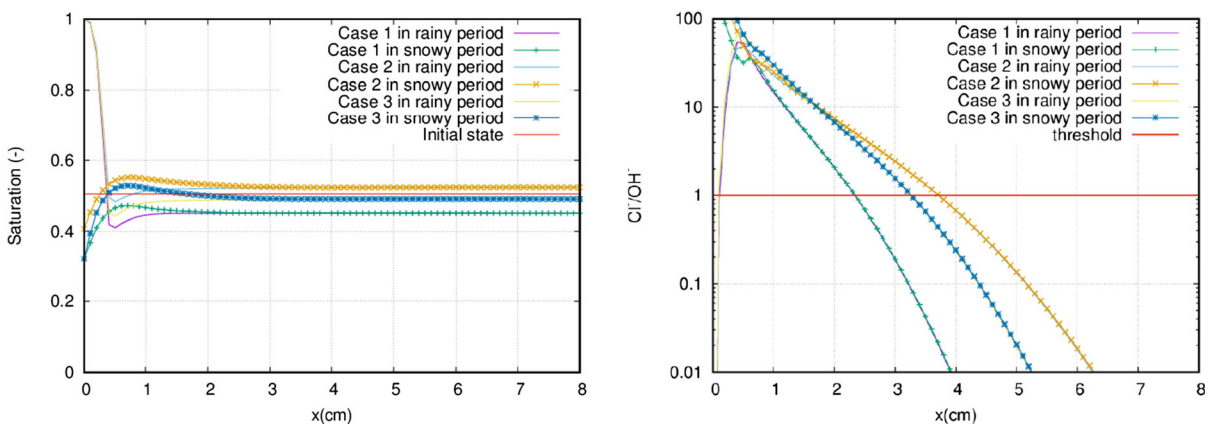

Fig. 4 Liquid saturation degree (left) and Cl^-/OH^- ratio (right) of Case 1–3 in 50 years without carbonation

calculate the carbonation depth and its effects on chloride ingress. Figure 5 provides the results on the carbonation depth, characterized by the consumption of CH and formation of calcite, and the porosity profiles. The final carbonation depth is in the range of 2–3 cm after 50 years of exposure in Case 1–3, and Case 1 shows the largest carbonation depth due to two reasons: the relative humidity in drying periods is lower (55%), compared to Case 2, and the drying durations are longer with less frequent rainy and snowy events, compared to Case 3.

The chloride ingress is calculated using the reactive transport model and considering the atmospheric carbonation. The results of free chlorides are given in Fig. 6 (left) with profiles after rainy periods. To better illustrate the impact of atmospheric carbonation on the chloride ingress, the results without carbonation in Sect. 3.2 are also added into Fig. 6. The global effect of carbonation is found to limit the chloride ingress. Actually, the carbonation impacts on the chloride transport through several mechanisms: the release of bound chlorides by consumption of C-S-H as absorbents, the decrease of porosity by calcite precipitation, and the release of free water to change the pore saturation. From the results in Fig. 6, it seems that the pore filling effect on decreasing chloride diffusivity dominates the other effects. Certainly, this observation is closely related to the pore filling calculation in Eq. (8) and the dependence of chloride diffusivity on porosity, which will be discussed further in the parametric analysis of transport properties.

When we turn to the steel corrosion indicator, Cl^-/OH^-, the carbonation does not show unique effect in Fig. 6 (right): it seems to promote the corrosion for Case 1, but decrease the corrosion risk for Case 2 and Case 3. It results from the combined effects from the moisture transport, the concurrent CO_2 transport in gas phases and chloride transport in liquid phase, and the solid–liquid equilibrium regulated continuously by carbonation reactions in Table 1. However, the carbonation does not change the order of criticality of corrosion for the three cases: Case 2 > Case 3 > Case 1, meaning the impact of carbonation will not be superior to that of snow/rain event count and relative humidity. It seems that the impact of carbonation on the corrosion risk should be circumstanced with specific environmental conditions.

4 Impact of intrinsic properties of concrete materials

4.1 Models for transport properties

The transport properties involved in the reactive transport model include CO_2 diffusivity, liquid permeability and chloride diffusivity, and their change by carbonation as well. The most fundamental parameter, common to all transport properties, is concrete porosity, which is also changed by carbonation through Eq. (8). The retained expressions for these properties are reviewed in the following. The CO_2 diffusivity takes the expression from Papadakis [35],

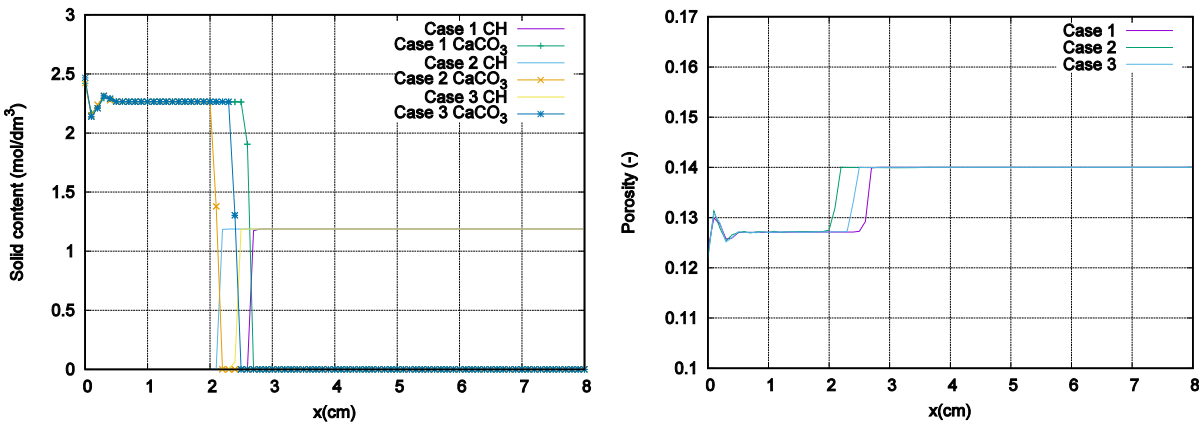

Fig. 5 Carbonation depth (left) and porosity (right) of Case 1–3 with natural carbonation in 50 years

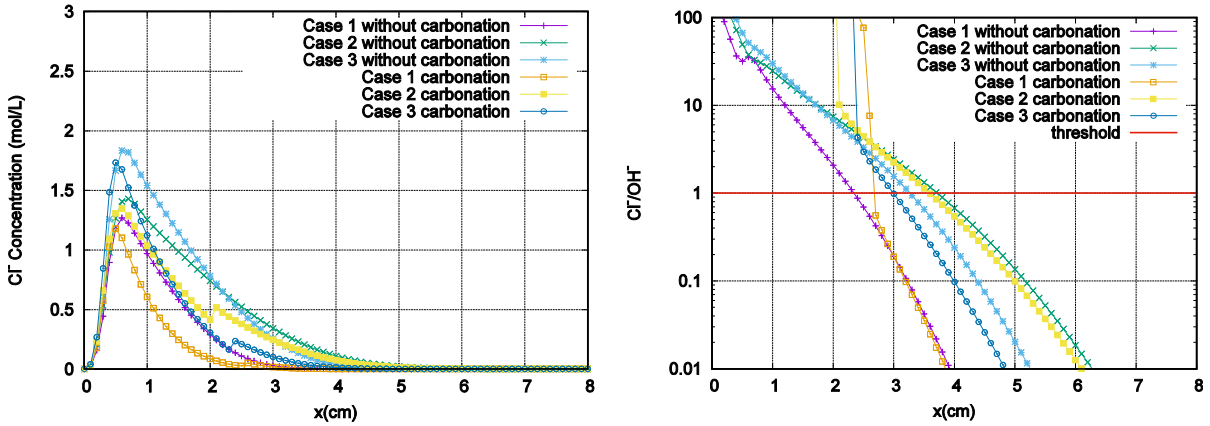

Fig. 6 Free chloride concentration in "rainy period" (left) and Cl^-/OH^- ratios (right) of Case 1–3 with and without carbonation in 50 years

$$D^{e}_{CO_2(G)} = 1.64 \times 10^{-6}\phi_p^{1.8}(1-h)^{2.2} \tag{12}$$

where ϕ_p refers to the (capillary) porosity for hardened cement paste in concrete. The liquid permeability takes the following relation to take into account the porosity change [36],

$$k_{int} = k^0_{int}\left(\frac{\phi}{\phi_0}\right)^3\left(\frac{1-\phi_0}{1-\phi}\right)^2 \tag{13}$$

with k^0_{int} referring to the initial intrinsic permeability, and ϕ_0, ϕ to the initial porosity and altered porosity respectively. The chloride diffusivity takes Yokozeki's model [37],

$$D^e_i = \frac{1-cv_{ca}}{1-dv_{fa}}v_p f(\phi_p)s_L^{\lambda}D^0_i \tag{14}$$

where $D_i^{e,0}$ stand for effective chloride diffusivities in concrete and in pore solution respectively, $v_{ca,fa}$ for the volumetric ratio of coarse aggregates and fine aggregates, v_p for volumetric ratio of cement paste in concrete, c, d for two tortuosity factors associated with coarse and fine aggregates, and λ for the exponent of pore saturation dependence. The tortuosity function for cement paste, $f(\phi_p)$, takes the following form [38],

$$f(\phi_p) = 0.001 + 0.07\phi_p^2 + 1.8(\phi_p - 0.18)^2\cdot H(\phi_p - 0.18) \tag{15}$$

where $H(\cdot)$ signifies the Heaviside function with $H(x) = 0$ as $x \le 0$ and $H(x) = 1$ as $x > 0$. Moreover, the long-term ageing of chloride diffusivity is taken into account [17], and the ageing factor is retained as $(t_0/t)^m$. All these material parameters can be found in Table 3 for the concretes used in the simulations.

4.2 Carbonation-altered transport properties

To address clearly how carbonation impacts on the chloride ingress through the transport properties change, several simulations are performed under Case 2 conditions with the concrete initial properties given in Table 3: only CO_2 diffusivity altered by carbonation, only chloride diffusivity altered by carbonation, only permeability altered by carbonation, and no transport properties altered by carbonation. The purpose of this group of simulations is to investigate how the carbonation-altered properties impact on the chloride ingress and also to identify the application scope of the results obtained in this study. The results of free chloride profiles are provided in Fig. 7 (left) and we add also the results of chloride ingress with and without carbonation from Fig. 6 and Fig. 3 in order to make a comprehensive comparison. The respective impact of these altered properties can be read from Fig. 7 (left): the case "without carbonation" has the highest chloride profile while the case "with carbonation" remains the lowest; the case "no transport properties altered" provides the pure chemical effect of carbonation on the chloride ingress; the case "chloride diffusivity altered" is responsible to the depressed chloride profiles after carbonation while the alteration of permeability and CO_2 diffusivity is not dominating. Note that all transport properties interplay

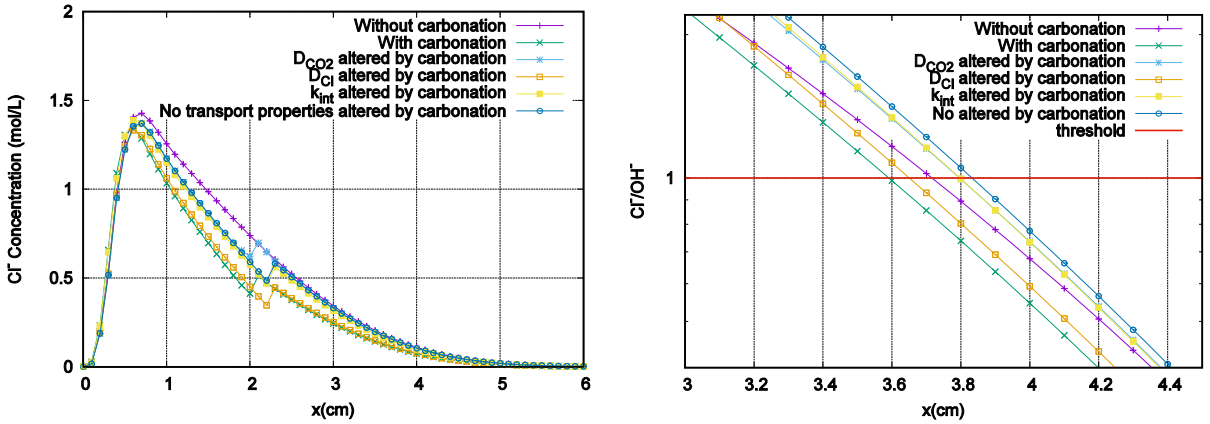

Fig. 7 Free chloride concentration with different input parameters in "rainy period" (left) and enlarged Cl^-/OH^- ratio (right) for Case 2 in 50 years

for carbonation depth and different carbonation depths are obtained from the different simulation cases.

The corrosion initiation indicator is evaluated for different simulation cases in Fig. 7 (right). From this figure, one can get more direct information on the respective impact of altered transport properties. First, the carbonation case has the smallest initiation depth while the case "no transport properties altered by carbonation" reaches the deepest depth, meaning that if no alteration is considered for transport properties the pure chemical effect of carbonation does increase the corrosion risk. The case "without carbonation" is in the middle, showing if taking into account of carbonation-altered properties the carbonation tends to limit the corrosion risk otherwise the risk will be promoted. The most "protective" effect of altered properties is attributed to the chloride diffusivity, and the altered CO_2 diffusivity and permeability are not protective with respect to corrosion risk. In other words, the obtained simulation results are rather sensitive to how these transport properties are altered by carbonation, especially the chloride diffusivity.

4.3 Composition of cementitious materials

Apart from the transport properties, the chemical composition of cement hydrates also has an important impact on the carbonation [39, 40]. So far, all simulations are performed on the OPC concrete with parameters provided in Table 3. This section is dedicated to complex binders incorporating fly-ash (FA), which is recommended for chloride ingress environments [41], and the impact of using FA as supplementary cementitious materials (SCM) in concrete binders under actions of de-icing salts. To this purpose, the environmental condition Case 2 is retained and three dosages of FA are taken into account in the simulations: 0, 10% and 20%. From the thermodynamic data for blended binders [42], the amount of carbonation reactants is determined for the concretes of OPC(0%FA), OPC+10%FA and OPC+20%FA, cf. Table 3. The ageing factor for chloride diffusivity for OPC-FA concretes is retained as 0.66 following [17], and other properties take the same values as OPC concrete in Table 3.

The carbonation results are given in Fig. 8, and the impact of incorporating FA into binder is clearly showed by the carbonation depth. With 20%FA in binder, the CH content deceases from 1085 to 63 mol/m^3, resulting in much less reactants for carbonation. The corresponding carbonation depth is nearly 1 cm more than the carbonation depth of 0%FA case. The chloride profiles are given in Fig. 9 (left) for free and total chloride concentrations. Since OPC + 20%FA concrete has less carbonation reactants, the pore filling effect is less pronounced than OPC+ 0%FA and OPC + 10%FA concretes, cf. Figure 8 (right). Recalling the main observation in the precedent section, this less important pore filling gives largest chloride diffusivity after carbonation, leading to the most advanced chloride ingress. Figure 9 (right) translates the results into the corrosion initiation indicator, giving the highest risk for the OPC + 20% FA case, i.e. the depth of 4 cm after exposure of

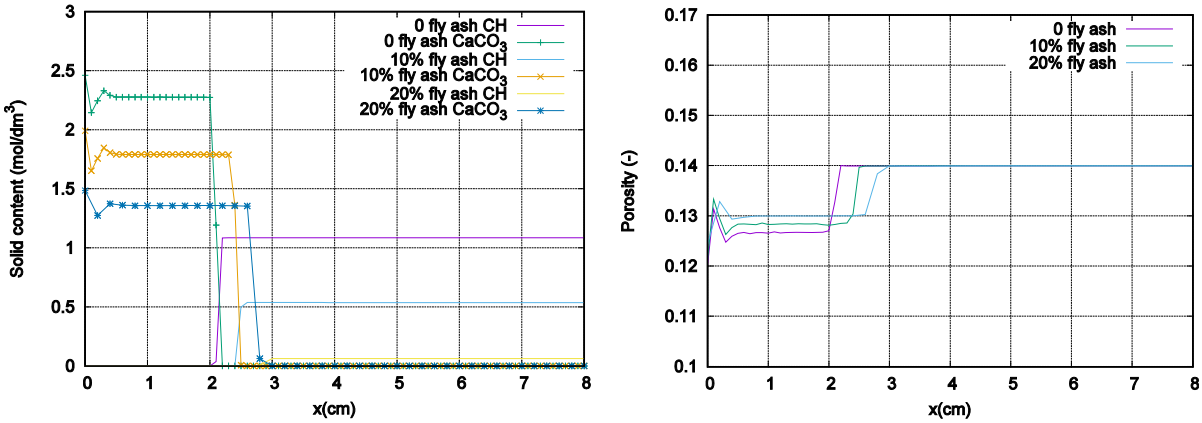

Fig. 8 Solid phase content (left) and porosity (right) for Case 2 with different cement (binder) composition with natural carbonation in "snowy period" in 50 years

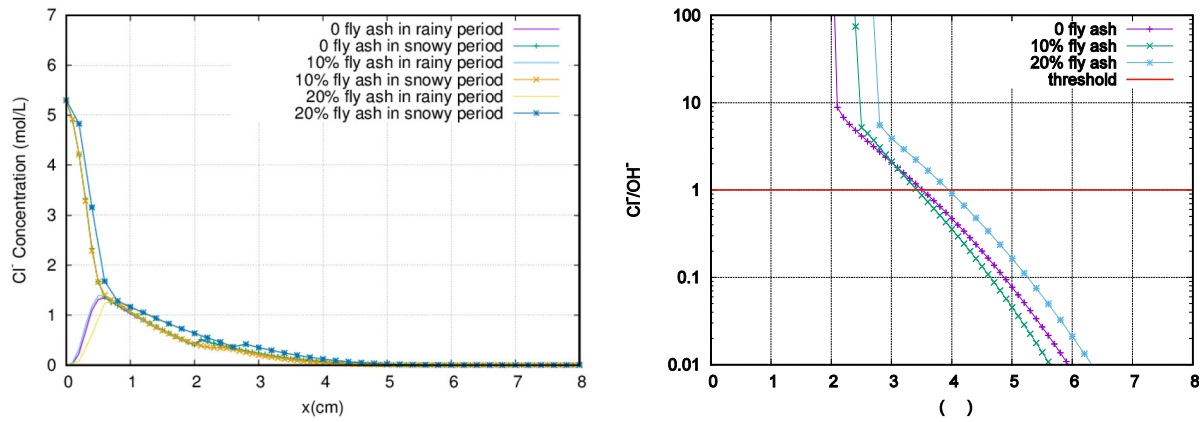

Fig. 9 Free chloride concentration (left) and Cl^-/OH^- ratios (right) of Case 2 with different chemical composition cements with natural carbonation in "snowy period" in 50 years

50 years. These results would imply that incorporating FA into binders will compromise the corrosion resistance of RC elements. However, it should be noted that in these simulation the same initial transport properties are used for all three concretes, and in practice the concrete mixtures containing FA will reduce intentionally the water to binder ratio for a same strength grade. Moreover, the long-term secondary hydration of FA can refine the pore structure of concretes and the contained alumina phases can promote the chemical binding (absorption) of chlorides. Thus, the above results should be interpreted with awareness that these beneficial effects from FA are not considered.

5 Further analysis on moisture conditions

We return to the modelling of moisture conditions on concrete surface. So far, the moisture conditions are defined with evenly distributed rainy or snowy events (RH = 100%) and intermittent drying periods (average RH). However, the atmospheric carbonation is more widely investigated with respect to a certain relative humidity without considering the rainy events or with a weather coefficient to address the influence of climates [43, 44]. This section is dedicated to the different prescriptions of moisture conditions with and without considering rain events. Here the dependence of chloride diffusivity D_i^e on pore saturation degree s_L is recalled as follow,

$$D_i^e = s_L^\lambda D_i \quad (16)$$

where D_i represents chloride diffusivity in saturated concrete and the exponent λ takes 6.0 following Nguyen [45]. The reactive transport model in Sect. 2 is used to calculate chloride ingress considering carbonation for different moisture boundary prescriptions for Case 2: cyclic raining events and different constant relative humidity (RH 65%, 67.5%, 70%, 72.5% and 75%) for rainy season.

The pore saturation and chloride profiles are given in Fig. 10 for different moisture conditions in 50 years. The adopted RH values are increased from the average RH = 65% to different extent to account for the wetting effect of intermittent rain events. From the pore saturation, the cyclic raining condition results in a global wetting effect while all constant RH values, except RH = 75%, lead to drying. In other words, if the global wetting effect is to be simulated, an equivalent relative humidity, higher than the value in equilibrium with the initial pore saturation, should be prescribed. From the chloride profiles, the constant RH boundary conditions, though giving a global drying for concrete, lead to much faster chloride ingress. The cyclic rainy boundary leads to more severe washing effect for chloride deposit on concrete surface, and this effect is missed by the constant RH boundary [46]. The corrosion indicator Cl^-/OH^- is also solved and presented in Fig. 11, and the corrosion initiation depth, measured by $Cl^-/OH^- = 1.0$, is rather sensitive to the RH boundary conditions. Higher RH conditions lead to deeper corrosion initiation depth and the depth from cyclic boundary is amid the results from different RH values.

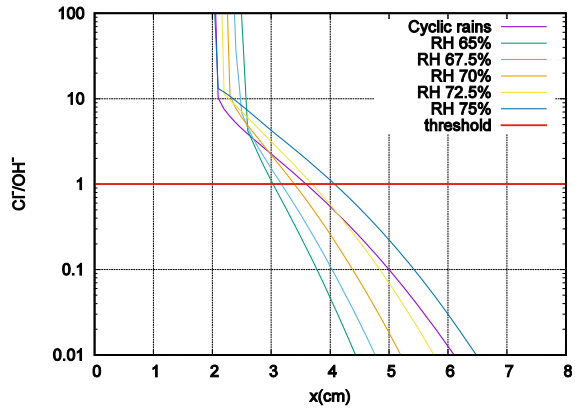

Fig. 11 Cl^-/OH^- ratios (Case 2) with different moisture conditions in 50 years

Summarizing the results of pore saturation, chloride profile and corrosion initiation indicators, one can see that the cyclic rainy events cannot be easily turned to equivalent constant RH values. Without accounting for the surface washing for chloride deposit, the constant RH boundary, even observing the global drying or wetting of concrete surface, tends to overestimate the chloride ingress. Note that the surface suction of concrete in direct contact with liquid water or solution involves complex flow behaviours [47, 48], the expression of capillary suction in the simulations, through Eqs. (2), (7), (10) and (11), should be calibrated further against concrete suction data to achieve more accurate prediction of moisture and chloride profiles under drying-wetting actions.

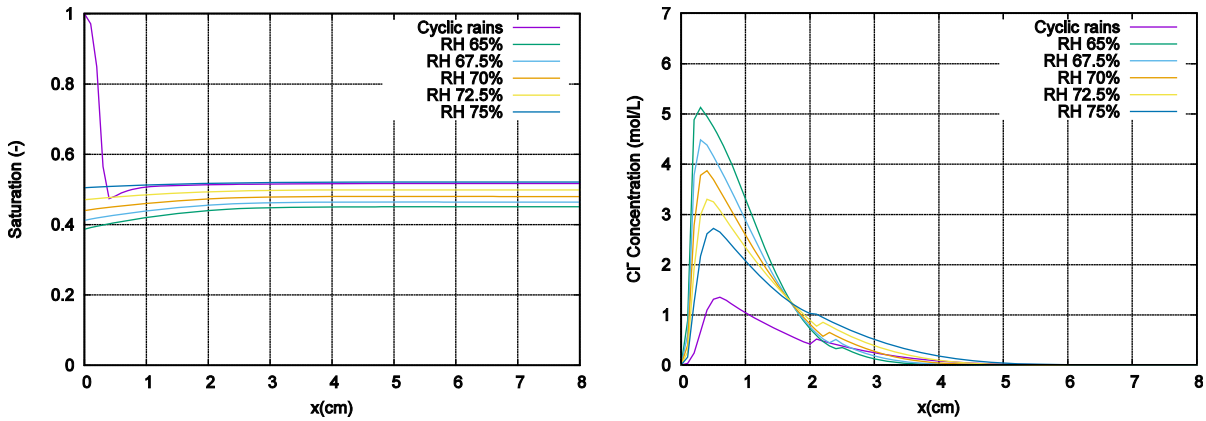

Fig. 10 Saturation degree (left) and free chloride concentration (right) with different relative humidity conditions in "rainy period" for Case 2 in 50 years

6 Conclusions

1. This paper attempts to investigate the chloride ingress into concrete under alternative actions of de-icing salts and atmospheric CO_2 through a comprehensive reactive transport modelling for concurrent ionic transport and carbonation in concrete. The reactive transport model takes into account the CO_2 diffusion, moisture transport and multi-species ionic transport in concrete pores, solid–liquid phase equilibrium, and the carbonation reactions. To simulate the environmental conditions of de-icing salts, the concrete surface is subjected to the intermittent de-icing salts related to snow events in "snowy period", to the intermittent surface wetting associated with raining events in "rainy period", and to the actions of atmospheric CO_2 during the dry durations. A such arrangement includes the main characteristics of boundary conditions of concrete surface.
2. Two typical climates, with frequent rainy and snowy events and less frequent ones, and a crossed case are retained for parametric analysis on the climate parameters of the chloride ingress. The chloride ingress under the yearly cyclic boundary conditions is first simulated without considering carbonation, showing that the intensity of de-icing salts application dominates over other factors and the relative humidity during drying periods plays a secondary role. The simulations considering carbonation show a global limiting effect of carbonation on the chloride ingress and corrosion initiation risk. From the further analysis on the moisture boundary conditions, the surface washing plays a central role in the chloride profiles near concrete surface and should be prescribed specifically on the concrete surface.
3. Another set of parametric analysis is performed on the impact of intrinsic properties and binder composition of concrete. The transport properties include CO_2 diffusivity, chloride diffusivity and intrinsic permeability, all depending on porosity. Without considering any alteration on the transport properties, the carbonation promotes the chloride ingress and the corrosion initiation risk as well. Considering all the alterations gives a global limiting effect of carbonation on chloride ingress and corrosion initiation risk, mainly due to the decrease of chloride diffusivity by pore filling after carbonation. Using the same initial porosity and transport properties as OPC concrete, the incorporation of FA into binders will decrease the carbonation reactants, thus promote the chloride ingress.
4. The simulation results obtained in this study are mainly for comparison purpose to clarify the impact of relevant factors on the chloride ingress from the action of de-icing salts, such as the intensity of de-icing salts application and the surface washing effect. The global limiting effect of carbonation on the chloride ingress is closely related to the sub-models of transport properties in terms of pore filling from carbonation. Being aware that these sub-models are far from universal, one should interpret this limiting effect with prudence, and other choices of these sub-models could alter this limiting effect. The same altitude should be borne for the simulation results for OPC-FA binders, which focus only on the consumption effect of CH without considering the possible pore refinement and chemical binding of chlorides by FA secondary hydration.

Funding This study is supported by NSFC Grant No. 51778332 and CSC scholarship (201706210326). This work is also a part of Innovandi partner project 31.1.

Declarations

Conflict of interest The authors declare that they have no conflict of interest.

References

1. Rivett MO, Cuthbert MO, Gamble R, Connon LE, Pearson A, Shepley MG, Davis J (2016) Highway deicing salt dynamic runoff to surface water and subsequent infiltration to groundwater during severe UK winters. Sci Total Environ 565:324–338. https://doi.org/10.1016/j.scitotenv.2016.04.095
2. Valenza JJ, Scherer GW (2007) A review of salt scaling: I. Phenomenol Cement Concrete Res 37(7):1007–1021
3. Valenza JJ, Scherer GW (2007) A review of salt scaling: II. Mech Cement Concrete Res 37(7):1022–1034
4. Jones C, Ramanathan S, Suraneni P, Hale WM (2020) Calcium oxychloride: A critical review of the literature surrounding the formation, deterioration, testing procedures, and recommended mitigation techniques. Cement Concr Compos. https://doi.org/10.1016/j.cemconcomp.2020.103663
5. Hussain SE, Rasheeduzzafar AA, Algahtani AS (1995) Factors affecting threshold chloride for reinforcement corrosion in concrete. Cement Concrete Res 25(7):1543–1555

6. CNS (2019) Code for durability design of concrete structures (GB/T50476–2019). China national standard, Beijing, China
7. ACI (2011) Building code requirements for structural concrete (ACI-318–11). American Concrete Institute, Farmington Hills, US
8. CEN (2002) Eurocode - Basis of structural design (EN1990:2002). European committee for standardization, Brussels, Belgium
9. Azad VJ, Li C, Verba C, Ideker JH, Isgor OB (2016) A COMSOL–GEMS interface for modeling coupled reactive-transport geochemical processes. Comput Geosci 92:79–89. https://doi.org/10.1016/j.cageo.2016.04.002
10. Isgor OB, Weiss WJ (2018) A nearly self-sufficient framework for modelling reactive-transport processes in concrete. Mater Struct. https://doi.org/10.1617/s11527-018-1305-x
11. Zhu X, Zi G, Lee W, Kim S, Kong J (2016) Probabilistic analysis of reinforcement corrosion due to the combined action of carbonation and chloride ingress in concrete. Constr Build Mater 124:667–680. https://doi.org/10.1016/j.conbuildmat.2016.07.120
12. Shen X-h, Liu Q-f, Hu Z, Jiang W-q, Lin X, Hou D, Hao P (2019) Combine ingress of chloride and carbonation in marine-exposed concrete under unsaturated environment: A numerical study. Ocean Eng. https://doi.org/10.1016/j.oceaneng.2019.106350
13. Xie M, Dangla P, Li K (2021) Reactive transport modelling of concurrent chloride ingress and carbonation in concrete. Mater Struct. https://doi.org/10.1617/s11527-021-01769-9
14. Tang L, Utgenannt P (2007) Chloride ingress and reinforcement corrosion in concrete under de-icing highway environment – a study after 10 years' field exposure. SP Report 2007:76. SP Technical Research Institute of Sweden, Borås, Sweden
15. Tang L, Lindvall A (2013) Validation of models for prediction of chloride ingress in concrete exposed in de-icing salt road environment. Int J Struct Eng. https://doi.org/10.1504/ijstructe.2013.050766
16. Kuosa H, Ferreira RM, Holt E, Leivo M, Vesikari E (2014) Effect of coupled deterioration by freeze-thaw, carbonation and chlorides on concrete service life. Cement Concrete Comp 47:32–40
17. DuraCrete (2000) Probabilistic performance based durability design of concrete structures. The European Union–Brite EuRam III, final technical report of Duracrete project, Document BE95-1347/R17. The Netherlands
18. Luping T (2008) Engineering expression of the ClinConc model for prediction of free and total chloride ingress in submerged marine concrete. Cement Concrete Res 38(8–9):1092–1097. https://doi.org/10.1016/j.cemconres.2008.03.008
19. Dangla P, Dridi W (2009) Rebar corrosion in carbonated concrete exposed to variable humidity conditions. Interpretation of Tuutti's curve Corros Sci 51(8):1747–1756. https://doi.org/10.1016/j.corsci.2009.04.029
20. Lothenbach B, Winnefeld F (2006) Thermodynamic modelling of the hydration of Portland cement. Cement Concrete Res 36(2):209–226. https://doi.org/10.1016/j.cemconres.2005.03.001
21. Greenberg SA, Chang TN (1965) Investigation of the colloidal hydrated calcium silicates II Solubility relationships in the calcium oxide-silica-water system at 25. J Phys Chem 69(1):182–188
22. Shen J, Dangla P, Thiery M (2013) Reactive transport modeling of CO2 through cementitious materials under CO_2 geological storage conditions. Int J Greenhouse Gas Control 18:75–87. https://doi.org/10.1016/j.ijggc.2013.07.003
23. van Genuchten MT (1980) A closed-form equation for predicting the hydraulic conductivity of unsaturated soils. Soil Sci Soc Am J 44(5):892–898. https://doi.org/10.2136/sssaj1980.03615995004400050002x
24. Mainguy M, Coussy O, Baroghel-Bouny V (2001) Role of air pressure in drying of weakly permeable materials. J Eng Mech 127(6):582–592. https://doi.org/10.1061/(asce)0733-9399(2001)127:6(582)
25. Dangla P (2018) A modeling platform based on finite volume/element method. https://github.com/ifsttar/bil
26. Cunningham MA, Snyder E, Yonkin D, Ross M, Elsen T (2007) Accumulation of deicing salts in soils in an urban environment. Urban Ecosystems 11(1):17–31. https://doi.org/10.1007/s11252-007-0031-x
27. Novotny EV, Murphy D, Stefan HG (2008) Increase of urban lake salinity by road deicing salt. Sci Total Environ 406(1–2):131–144
28. Trenouth WR, Gharabaghi B, Perera N (2015) Road salt application planning tool for winter de-icing operations. J Hydrol 524:401–410
29. Hossain SMK, Fu LP, Lu CY (2014) Deicing performance of road salt modeling and applications. Transport Res Rec 2440:76–84
30. China Meteorological Data Service Centre (2021) http://data.cma.cn/
31. Li K, Pang X, Dangla P (2016) Thermo–hydro-ionic transport in sea immersed tube tunnel. Tunn Undergr Space Technol 58:147–158. https://doi.org/10.1016/j.tust.2016.05.004
32. Baroghel-Bouny V, Mainguy M, Lassabatere T, Coussy O (1999) Characterization and identification of equilibrium and transfer moisture properties for ordinary and high-performance cementitious materials. Cement Concrete Res 29(8):1225–1238
33. Kayyali OA, Haque MN (1995) The C1−/OH−ratio in chloride-contaminated concrete — a most important criterion. Mag Concr Res 47(172):235–242. https://doi.org/10.1680/macr.1995.47.172.235
34. Florides GA, Christodoulides P (2009) Global warming and carbon dioxide through sciences. Environ Int 35(2):390–401. https://doi.org/10.1016/j.envint.2008.07.007
35. Papadakis VG, Vayenas CG, Fardis MN (1991) Physical and chemical characteristics affecting the durability of concrete. Aci Mater J 88(2):186–196
36. Carman PC (1937) Fluid flow through granular beds. Trans Inst Chem Eng 15:150–166
37. Yokozeki K, Watanabe K, Sakata N, Otsuki N (2004) Modeling of leaching from cementitious materials used in underground environment. Appl Clay Sci 26(1–4):293–308. https://doi.org/10.1016/j.clay.2003.12.027
38. Garboczi EJ, Bentz DP (1992) Computer simulation of the diffusivity of cement-based materials. J Mater Sci 27(8):2083–2092. https://doi.org/10.1007/bf01117921

39. Shah V, Bishnoi S (2018) Carbonation resistance of cements containing supplementary cementitious materials and its relation to various parameters of concrete. Constr Build Mater 178:219–232. https://doi.org/10.1016/j.conbuildmat.2018.05.162
40. Saillio M, Baroghel-Bouny V, Pradelle S, Bertin M, Vincent J, d'Espinose de Lacaillerie J-B (2021) Effect of supplementary cementitious materials on carbonation of cement pastes. Cement Concrete Res. https://doi.org/10.1016/j.cemconres.2021.106358
41. Polder RB, Peelen WHA (2002) Characterisation of chloride transport and reinforcement corrosion in concrete under cyclic wetting and drying by electrical resistivity. Cement Concr Compos 24(5):427–435. https://doi.org/10.1016/s0958-9465(01)00074-9
42. Lothenbach B, Scrivener K, Hooton RD (2011) Supplementary cementitious materials. Cement Concrete Res 41(12):1244–1256. https://doi.org/10.1016/j.cemconres.2010.12.001
43. Yoon IS, Copuroglu O, Park KB (2007) Effect of global climatic change on carbonation progress of concrete. Atmos Environ 41(34):7274–7285
44. Fib (2006) Model Code for Service Life Design, fib Bulletin 34. Federation Internationale des Bétons, Lausanne
45. Nguyen TQ (2007) Modélisations physico-chimiques de la pénétration des ions chlorures dans les matériaux cimentaires. École nationale des ponts et chaussées (France)
46. Hong K, Hooton RD (2000) Effects of fresh water exposure on chloride contaminated concrete. Cement Concrete Res 30(8):1199–1207
47. Lunk P (1998) Penetration of water and salt solutions into concrete by capillary suction. J Restorat Build Monuments 4(4):399–422
48. Li KF, Li CQ (2013) Modeling hydroionic transport in cement-based porous materials under drying-wetting actions. J Appl Mech ASME 80(3):020904